

# RAMAN STUDY ON THE PROCESS OF SI ADVANCED INTEGRATED CIRCUITS

S. Nishibe, T. Sasaki and H. Harima  
Kyoto Institute of Technology, Matugasaki, Kyoto 606-8585, Japan  
K. Kisoda  
Wakayama University, Sakaedani, Wakayama 640-8510, Japan  
T. Yamazaki and W.S. Yoo  
WaferMasters, Inc., San Jose, California 95112, U.S.A.

Precise control of fabrication processing is a key point for future integration technology of Si devices. Reliable characterization of Si wafers at each fabrication process is indispensable. Raman scattering has high-potential as a technique for non-contact and nondestructive characterization which yields valuable information on Si-based materials. Here, a patterned Si wafer for a modern electronic device is characterized by Raman microprobe to study the effect of different processes on residual stress, as well as other physical aspects.

## INTRODUCTION

High reproducibility of advanced electronic device is obtained in production by a combination of modern processing technology and high-quality characterization techniques for finding the problems in processing materials to enable quick feedback of solutions. For example, shallow trench isolation (STI) structures, which are common elements in modern integrated circuits, are often accompanied by stress concentration in the periphery of the buried thick oxide layers. The concentrated stress may cause unexpected effects in final products, leading to serious deterioration of device performance or reliability.

Microscopic Raman scattering can be a powerful tool in characterizing device structures non-destructively. In principle, Raman scattering needs no sample preparation and brings us, depth-dependent information if we employ multiple probe-laser wavelengths with different sample penetration depths.

In this study, we will first briefly review basic aspects of Raman scattering with emphasis on the effects of crystalline imperfections, then report a Raman analysis on patterned Si wafers processed for integrated circuits. We will focus our attention mainly on the residual stresses induced by annealing and lattice damage due to an etching process.

## RAMAN SPECTRA OF PHONON INTERACTIONS

Raman scattering is an inelastic light scattering process by various elementary excitations in solids such as phonons. To first-order, Raman scattering by

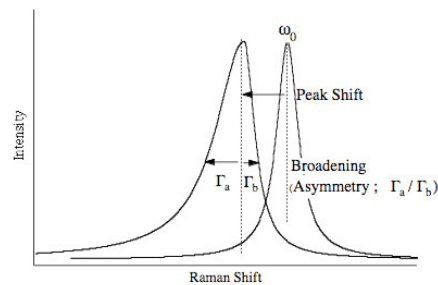


Fig. 1. Raman phonon peak. The ideal peak at frequency  $\omega_0$  is shifted and asymmetrically broadened by various factors.

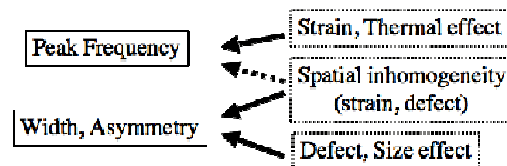


Fig. 2. Typical factors affecting Raman phonon peak.

phonons, yields a frequency difference between the incident and scattered photon, *i.e.*, Raman shift, gives the relevant phonon frequency at the  $\Gamma$ -point in the Brillouin zone. In the ideal case of bulk crystal Si, the  $\Gamma$ -point phonon is triply degenerate, and the Raman spectrum consists of a single Lorentzian peak located at  $520.3 \text{ cm}^{-1}$  with full width at half maximum (FWHM) of  $\sim 3 \text{ cm}^{-1}$ . However, in reality, the peak usually broadens, shifts in frequency and takes asymmetric line shape as shown schematically in Fig. 1. There are various factors affecting the spectral line

shape which can provide useful information; residual stress, thermal expansion, lattice defect, crystal-size effect *etc.* Figure 2 shows the causal relationship in a rough manner.

Residual stress is often the dominating factor for the peak shift. For example, if we observe the Si (100) plane under biaxial compressive stress by back scattering, the phonon peak will show a frequency up-shift  $\Delta\omega$  ( $\text{cm}^{-1}$ ) proportional to the sum of in-plane stress components  $\sigma_{xx} + \sigma_{yy}$  (MPa) [1],

$$\sigma_{xx} + \sigma_{yy} = 434 \Delta\omega. \quad (1)$$

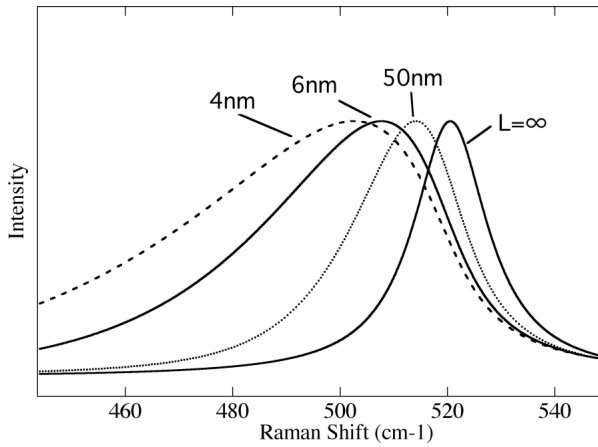


Fig. 3. Simulation of Raman phonon peak of Si. The peak down-shifts and asymmetrically broadens as the crystallite size  $L$  decreases.

However, if the plane is exposed to tensile stress, a frequency down-shift will be observed.

Small size crystals, typically of nm-order, exhibit very different behavior in Raman spectra from that of bulk crystals. Figure 3 shows a simulation Si phonon peak variation by the phonon confinement model [2]. As the crystallite size  $L$  decreases, the peak shows a frequency down-shift and is broadened with a tail to the lower frequency side. This effect becomes prominent roughly at  $L < 10$  nm. This variation has been actually observed in many examples of Si nanocrystals. Even bulk Si samples show similar variation when damaged by ion-implantation [3]. In that case, the crystallite size,  $L$ , corresponds to dimension of the damage-free region. Therefore, spectral broadening and asymmetry is enhanced as the lattice damage increases.

## EXPERIMENT

Here we examined Si 300-mm $\phi$  wafers patterned for an actual modern device (integrated circuit) at different processing stages; STI, annealing and gate-electrode formation. A standard experimental setup for microscopic Raman scattering was used for this purpose. As shown in Fig. 4, an Ar-gas laser at wavelength 514.5 nm was focused by an objective lens with magnification 10x and NA (numerical aperture) = 0.3, to a beam width of  $\sim 2$   $\mu\text{m}$  on a sample surface.

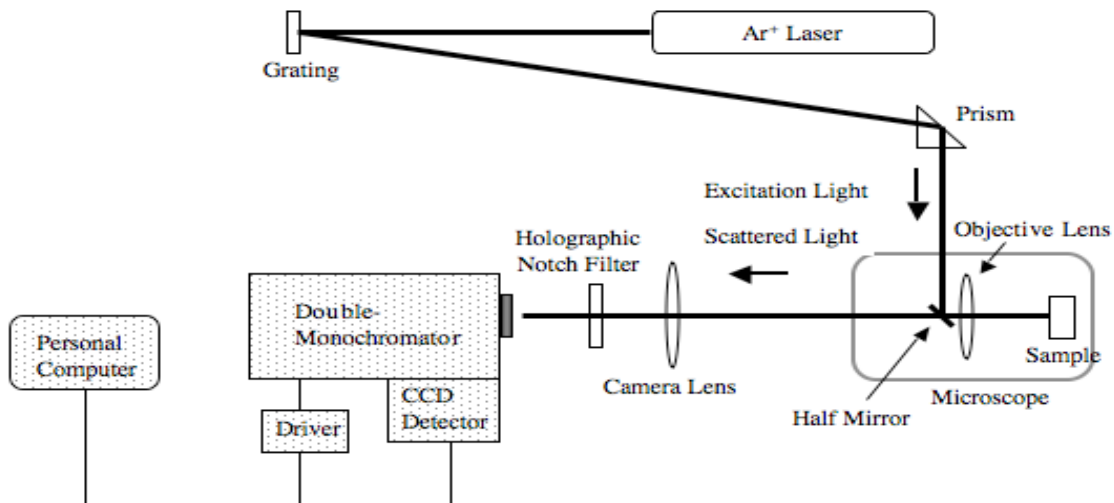


Fig.4 Setup of Raman microprobe.

The depth of the probed region is estimated from the absorption coefficient of the laser, to be  $\sim 350$  nm. The scattered light was collected by the same objective lens and collected at the entrance slit of a double monochromator equipped with a liquid-N<sub>2</sub>-cooled charge-coupled-device (CCD) detector. The incident laser (Rayleigh) component was rejected by a notch filter in front of the entrance slit.

To begin, we determined the suitable power of the probe laser because excessive power will cause lattice expansion due to heating. The peak frequency of Si was observed by varying the incident laser power for a wafer after an STI process. This wafer was used because it was most easily heated in the treated samples. As shown in Fig. 5, the peak showed a systematic frequency down-shift with increased input power. Throughout the present study, we chose  $\sim 1 \times 10^{-8}$  mW/cm<sup>2</sup> as a trade off between excessive lattice heating and saving measuring time.

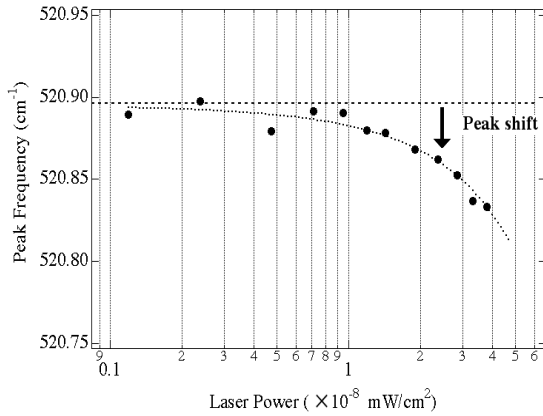


Fig. 5. Frequency of Si phonon peak at various incident laser power densities on sample surface.

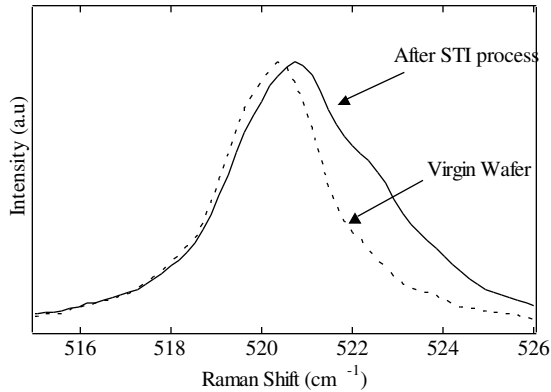


Fig. 6. Si phonon peak before processing (= virgin, dotted line) and after STI (solid line).

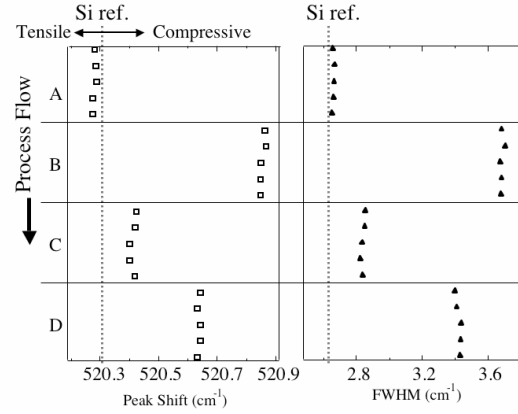


Fig. 7. Comparison of Si phonon peak frequency (open square) and FWHM (filled triangle) on wafers at different processing stages. The processing proceeds from top to bottom; (A) control, (B) STI, (C) annealing and (D) gate-electrode formation.

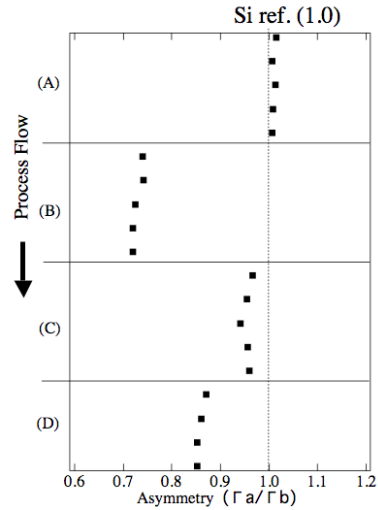


Fig. 8. Evolution of Si phonon peak asymmetry  $\Gamma_a/\Gamma_b$  as defined in Fig. 1. The processing proceeds from top to bottom.

In Fig. 6, the Si phonon peak is compared before STI formation (virgin wafer; as a control, dotted line) and after (solid line). The peak frequency is up-shifted after STI compared to the control, and broadened with a tail to the higher frequency side. This measurement was repeated at several points on a wafer at different processing stages, and the peak frequency and full width at half maximum (FWHM) were compared as shown in Fig. 7. Here, the process flows from top to bottom in the order of (A) control wafer, (B) STI processed, (C) annealing, and (D) formation of gate

electrode. The influence of each process on the wafer is clearly observed. Compared to the control wafer, the phonon peak is broadened and frequency is up-shifted by the STI process. These features are almost reversed by annealing and then enhanced again by gate-electrode formation. Figure 8 shows the change of peak asymmetry  $\Gamma_a/\Gamma_b$ , where  $\Gamma_a$  is the half width at half maximum (HWHM) to the lower frequency side and  $\Gamma_b$  the counterpart to higher frequency (see Fig. 1). The asymmetric feature becomes evident after STI, but is reversed by annealing, and enhanced again by gate-electrode formation.

## DISCUSSION

Here we will analyze the results shown in Figs. 7 and 8. As described in section 2, residual stress is the dominant cause for the peak-frequency shift; the peak shifts to higher frequency when the stress is compressive and to lower frequency for tensile stress. The peak-frequency variation in Fig. 7 clearly shows that a compressive stress is generated by the STI process, is reversed by annealing and re-generated by gate-electrode formation.

Increase in peak width can be interpreted roughly in two ways: Lattice defect induces shortening of phonon lifetime, leading to broadening of the Lorentzian phonon peak. If the lattice ordering is further deteriorated by damage, the peak shows appreciable frequency down-shift together with tailing to lower frequency, just like the crystalline size effect (see Fig. 4). If, on the other hand, the peak tails to higher frequency, existence of a spatially inhomogeneous distribution of compressive stress, is considered for the probed region. The observed features of peak broadening and asymmetry from the control wafer to STI suggest the latter mechanism.

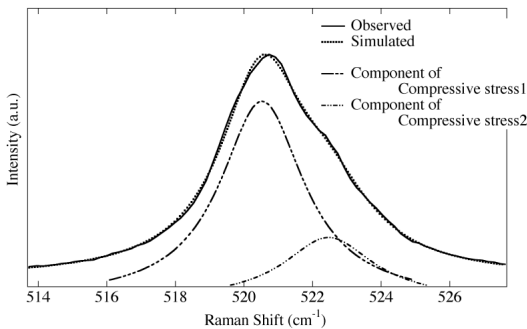


Fig. 9. Comparison of simulated profile (dotted line) with the observed (solid line). The two components with different compressive stress (dashed line) are assumed.

To confirm this speculation, we have simulated a peak profile by assuming a two-zone scheme and compared it with the observed profile shown in Fig. 5. Here, the probed Si region consists of two regions; one is compressed in-plane by 200 MPa and the other by 850 MPa; their volume ratio is 4:1. These stresses will induce a peak frequency up-shift of  $0.5 \text{ cm}^{-1}$  and  $2 \text{ cm}^{-1}$ , respectively, according to Eq. (1). Summing these components, the resultant profile (dotted line in Fig. 9) almost reproduces the observed feature (solid line). To get better agreement for the high frequency tail, we have to assume a distribution of compressively-stressed regions as shown schematically in Fig. 10, where the stress decreases continuously with depth, from the surface of the Si wafer.

The stress distribution speculated in Fig. 10 is derived from the patterned surface structure after an STI process: The difference in thermal expansion coefficients between Si and  $\text{SiO}_2$  probably plays an important role. A more detailed analysis, such as depth-sensitive analysis using different penetration depths of probe lasers will clarify the situation.

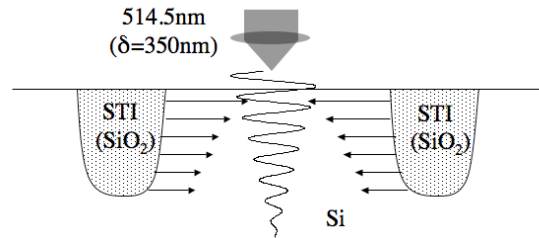


Fig. 10. Inhomogeneous stress distribution. (as suggested from Fig. 9.)

## SUMMARY

Silicon wafers, patterned for integrated circuits, were characterized by microscopic Raman scattering at different processing stages; shallow trench isolation (STI), annealing, and gate-electrode formation. We have observed characteristic variations of the Si phonon peak in the peak width, frequency and asymmetry. The results suggested generation of an inhomogeneous distribution of a compressively stressed region after STI process, which was reversed by annealing and re-generated by electrode formation.

Since, in this experiment, we used only one laser wavelength 514.5 nm, the probed region is limited to the penetration depth,  $d \sim 350 \text{ nm}$ . If we choose different lasers of wavelength, e.g., 457.9 nm ( $d \sim 140 \text{ nm}$ ) and 363.8 nm ( $d \sim 5 \text{ nm}$ ), we could observe more

details with depth of Si wafer. Thus, Raman scattering will be a much more powerful, non-contact characterization method to trace the effects of processing on wafers, and to improve the device yield by providing quick feedback of the data to process engineers.

#### ACKNOWLEDGEMENT

We would like to express my gratitude to Dr. K. Ohyu and Mr K. Okonogi of Elpida Memory, Inc. for supplying the samples and useful discussions.

#### REFERENCES

- [1] D. Wolf, *J. Raman Spectrosc.* 30 (1999, 1) 877-833.
- [2] I.H.Campbell and P.M.Fauchet, *Solid State Comm.* 58 (1986) 739.
- [3] X.Huang, F.Ninio, L.Brown, and S.Prawer, *J. Appl. Phys.* 77 (1995) 5910.